Numerical study of multistage transcritical ORC axial turbines

L. Sciacovelli, P. Cinnella

Laboratoire DynFluid - Arts et Métiers ParisTech
151 Boulevard de l'Hôpital, 75013 Paris

08 October 2013

Table of Contents

Context

- Supercritical ORCs are a promising improvement for ORC technology

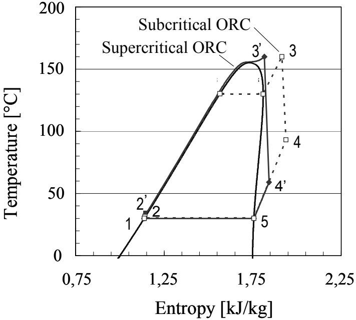

Comparison sub- and supercritical ORCs. [Karellas and Schuster, 2010]

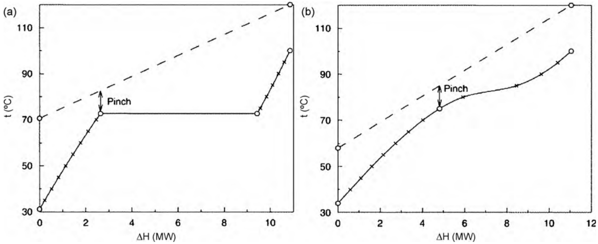

Heating phase for an organic fluid at sub- and supercritical pressure. [Saleh et al., 2007]

Advantages:

- Higher thermal and heat recovery efficiencies
- Better thermal match in the heat exchanger
- Simplified cycle architecture

Problems:

- Higher pressures, higher costs
- Difficulties in modelling the fluid in the critical region

Thermodynamic Modelling

Candidate working fluids: R134a, R245fa, CO_2

- Dense gas behavior modeled through EoS based on **Helmholtz free energy** Φ
  - Reduced parameters $\delta = \rho/\rho_c$ and $\tau = T_c/T$ as indipendent variables
  - EoS composed by ideal and residual part

$$\Phi(\delta, \tau) = \Phi^0(\delta, \tau) + \Phi^r(\delta, \tau)$$

$$\Phi^0(\delta, \tau) = \ln \delta + a_1 \ln \tau + \sum_{m=1}^{M_1} a_m \tau^{j_m} + \sum_{m=M_1+1}^{M_2} a_m \ln[1 - \exp(-u_m \tau)]$$

$$\Phi^r(\delta, \tau) = \sum_{m=M_2+1}^{M_3} a_m \delta^{i_m} \tau^{j_m} + \sum_{m=M_3+1}^{M_4} a_m \delta^{i_m} \tau^{j_m} \exp(-\delta^{k_m}) + \sum_{m=M_4+1}^{M_5} a_m \delta^{i_m} \tau^{j_m} \exp[-\alpha_m (\delta - \epsilon_m)^2 - \beta_m (\tau - \gamma_m)^2]$$

- The ideal part requires an ancillary equation for the ideal-gas heat capacity
- Coefficients, exponents and number of terms calibrated on experimental data by means of an optimization algorithm [Setzmann and Wagner, 1989]

Thermodynamic Modelling

- Reference EoS available only for R134a and CO_2. For R245fa, the Span-Wagner short technical multiparameter EoS has been used
  - The ideal part $\Phi^0(\delta,\tau)$ conserves the same form
  - Less accurate w.r.t. the complete EoS, due to the smaller experimental data bank available

$$\begin{aligned}\Phi^r(\delta,\tau) = n_1\delta\tau^{0.25} &+ n_2\delta\tau^{1.25} + n_3\delta\tau^{1.5} + \\ &+ n_4\delta^3\tau^{0.25} + n_5\delta^7\tau^{0.875} + n_6\delta\tau^{2.375}\exp(-\delta) + \\ &+ n_7\delta^2\tau^{2.0}\exp(-\delta) + n_8\delta^5\tau^{2.125}\exp(-\delta) + \\ &+ n_9\delta\tau^{3.5}\exp(-\delta^2) + n_{10}\delta\tau^{6.5}\exp(-\delta^2) + \\ &+ n_{11}\delta^4\tau^{4.75}\exp(-\delta^2) + n_{12}\delta^2\tau^{12.5}\exp(-\delta^3)\end{aligned}$$

- Fluid viscosity μ and thermal conductivity κ evaluated using the relations described in [Chung et al., 1988]:

$$\mu = 40.785\frac{F_c M_w^{1/2} T^{1/2}}{V^{2/3}\Omega_v} \qquad \frac{\kappa M_w}{\mu C_v} = \frac{3.75\Psi}{C_v/R}$$

Numerical method

Equations of motion:

$$\int_{\Omega(t)} \boldsymbol{\omega}\, d\Omega + \oint_{\partial\Omega(t)} (\mathbf{f}^e - \mathbf{f}^v)\cdot\mathbf{n}\, dS = \mathbf{s}, \qquad \boldsymbol{\omega} = \begin{bmatrix} \rho \\ \rho\mathbf{v} \\ \rho E \end{bmatrix} \mathbf{f}^e = \begin{bmatrix} \rho\mathbf{v} \\ \rho\mathbf{v}\mathbf{v} + p\mathbf{I} \\ \rho\mathbf{v}H \end{bmatrix} \mathbf{f}^v = \begin{bmatrix} 0 \\ \boldsymbol{\tau} \\ \boldsymbol{\tau}\cdot\mathbf{v} - \mathbf{q} \end{bmatrix}$$

with $p = p(e(\omega), \rho(\omega))$ or

Caloric EoS: $e = e(T(\omega), \rho(\omega))$

Thermal EoS: $p = p(T(\omega), \rho(\omega))$

Spatial discretization:

- Structured finite-volume approach
- Third-order accuracy, centered, conservative scheme with artificial viscosity
- Extension to curvilinear grid using weighting coefficients that take into account mesh deformations

Time integration:

- Four-stage Runge-Kutta method with implicit residual smoothing

Turbulence modeling:

- Algebraic Model: *Baldwin-Lomax*
- One-equation Model: *Spalart-Allmaras*

Simulation setup

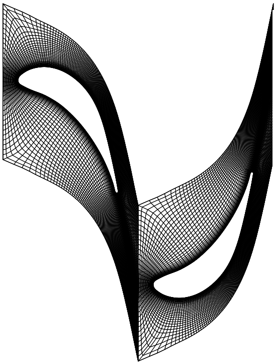

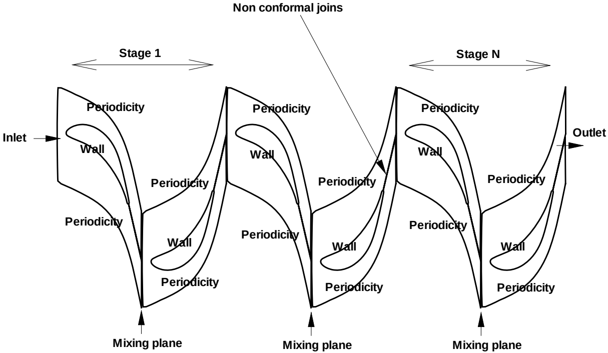

- Mesh composed by C-blocks
- Inviscid model: 273x33 points
- Viscous model: 389x49 points
- $y^+ = 1$

- Distances upstream and downstream the blades respectively equal to 0.15c and 0.2c, being c the axial chord

Gap between rotor and stator: *0.35c*

Simulation setup

R134a

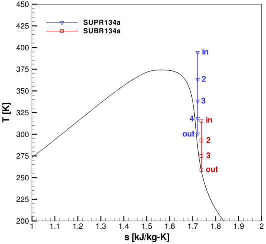

R245fa

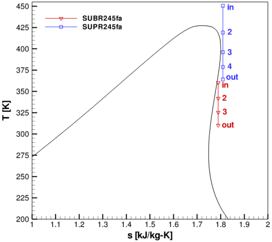

CO_2

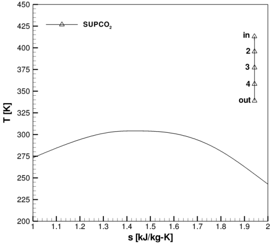

- Both sub- and supercritical admission conditions for R134a and R245fa
- Supercritical admission conditions only for CO_2 (light, wet fluid)

Parameters	SUBR134a	SUBR245fa	SUPR134a	SUPR245fa	$SUPCO_2$
p0 (bar)	10.4	9.5	47.1	46.9	150.5
T0 (K)	315.51	370.15	396.57	450.43	416.21
Stages	3	3	4	4	4
β_1	1.832	1.840	1.703	1.706	1.214
β_2	1.819	1.823	1.630	1.652	1.229
β_3	1.836	1.838	1.596	1.605	1.242
β_4	-	-	1.586	1.593	1.258
β_{tot}	6.118	6.165	7.026	7.208	2.331

Results: inviscid model

Turbine stage efficiencies for the inviscid model.

Stage	SUBR134a	SUBR245fa	SUPR134a	SUPR245fa	SUPCO_2
1	95.07	92.55	94.63	91.12	98.72
2	94.03	89.59	95.80	91.99	98.27
3	92.94	88.36	95.87	92.45	99.86
4	-	-	98.41	93.62	99.11

- Different isentropic efficiencies mainly due to different fluid dynamic behaviour
- Important parameter to evaluate the results: *Fundamental derivative of Gas Dynamics* [Thompson, 1971]:

$$\Gamma = 1 + \frac{\rho}{a}\left(\frac{\partial a}{\partial \rho}\right)_s \Rightarrow \frac{\partial a}{a} = (\Gamma - 1)\frac{\partial \rho}{\rho}$$

Results: viscous model

Turbine stage efficiencies for the B-L model.

Stage	SUBR134a	SUBR245fa	SUPR134a	SUPR245fa	SUPCO_2
1	84.21	78.55	85.72	82.04	89.67
2	83.99	78.41	86.23	82.15	89.91
3	83.86	77.28	86.91	82.56	90.04
4	-	-	87.64	82.99	90.11

Turbine stage efficiencies for the S-A model.

Stage	SUBR134a	SUBR245fa	SUPR134a	SUPR245fa	SUPCO_2
1	84.13	80.61	84.68	81.98	89.63
2	83.87	78.76	85.98	82.13	89.85
3	83.45	76.21	86.24	82.23	89.92
4	-	-	87.53	82.35	90.04

- Efficiencies about 10% lower w.r.t inviscid case
- Baldwin-Lomax predicts an efficiency about 1% higher than Spalart-Allmaras

Turbulence model comparison - R134a 1^{st} stage rotor

- Wall pressure on suction side slightly lower for B-L model
- Friction Coefficient higher for S-A model

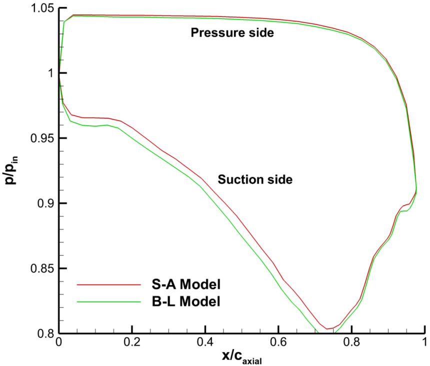

Dimensionless wall pressure

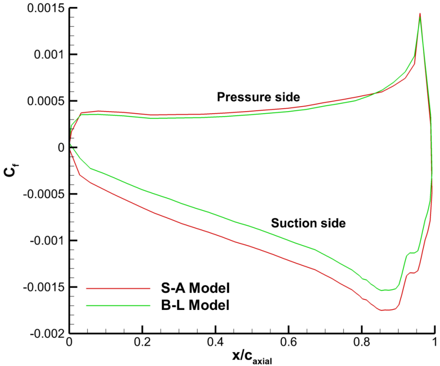

Friction coefficient

- Overall S-A efficiency lower
- Results presented in the following are computed with B-L

Results: SUPR134a case

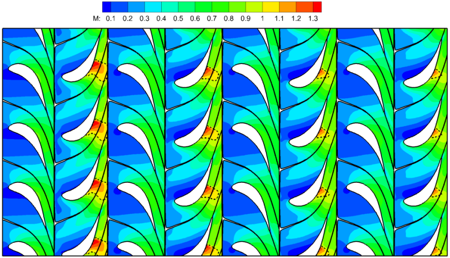

Relative Mach Number

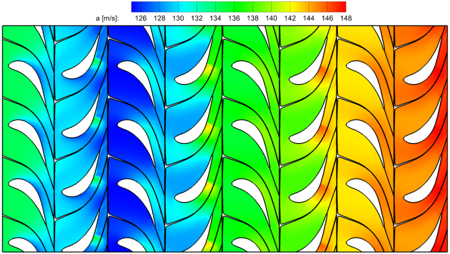

Sound speed

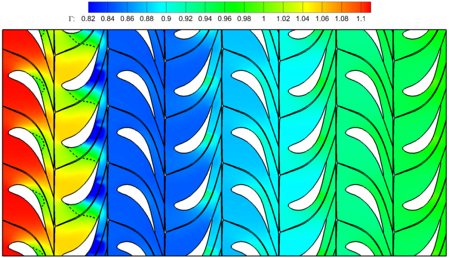

Fundamental Derivative of Gas Dynamics

- Presence of a weak shock at each rotor upper side, decreasing moving downstream
- I stage: Γ decreases but stays close to 1, thus sound speed nearly constant
- II-IV stage: $\Gamma < 1$, relative sound speed variation positive
- The higher the sound speed, the weaker the shocks

Results: SUBR245fa vs SUBR134a

- $\Gamma \approx 1$
- Sound speed nearly constant
- Stronger shocks
- Lower efficiencies

- Better behavior for R134a

R245fa

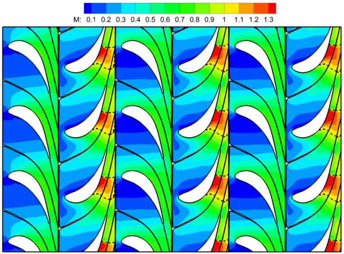

Relative Mach Number

R134a

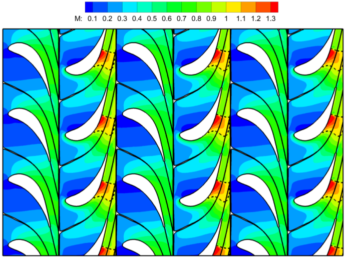

Relative Mach Number

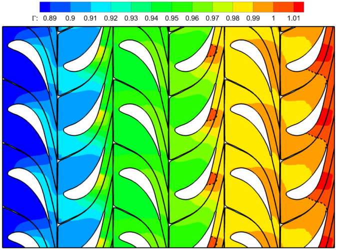

Fundamental Derivative of Gas Dynamics

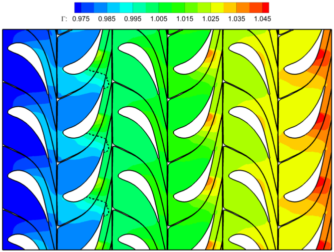

Fundamental Derivative of Gas Dynamics

Results: $SUPCO_2$ case

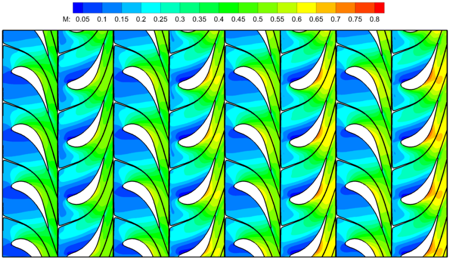

Relative Mach Number

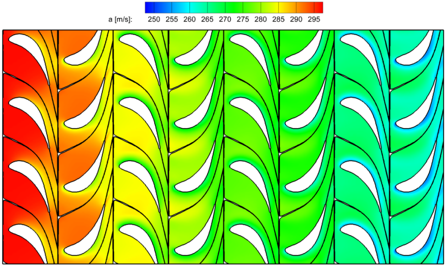

Sound speed

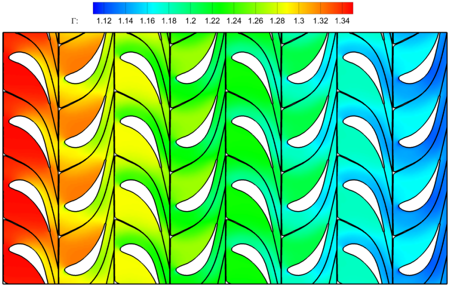

Fundamental Derivative of Gas Dynamics

- Supercritical expansion, $\Gamma > 1$ always
- Light fluid: high sound speed
- Absence of shocks: maximum efficiency in viscous and inviscid cases
- Higher plant costs due to higher mean pressures of the cycle

Conclusions and perspectives

Conclusions:

- In all the test cases performed, transcritical and supercritical admission conditions allowed to increase the turbine isentropic efficiency
- Overall efficiencies are globally about 10% lower than inviscid ones
- Viscous and inviscid models provide similar flow evolutions, due to the absence of recirculation zones and unsteady effects being neglected
- The B-L and S-A turbulence models predict similar results in terms of overall efficiency and evolution of thermodynamic variables
- CO_2 has the best fluid dynamic behavior, but also higher plant costs
- R134a ensures satisfactory adiabatic efficiencies, despite the presence of weak shocks at the suction sides of the rotor blades
- R245fa develops stronger shocks for the same configuration, leading to higher losses
- SUPR134a is the best compromise between fluid dynamic behavior and plant requirements for the ORC.

Perspectives:

- 2D unsteady simulations in order to evaluate wakes and transient effects
- 3D viscous simulations

THANKS FOR THE ATTENTION

References

Chen, H., Goswami, D., and Stefanakos, E. (2010). A review of thermodynamic cycles and working fluids for the conversion of low-grade heat. *Renewable and Sustainable Energy Reviews*, 14(9):3059–3067.

Chung, T. H., Ajlan, M., Lee, L. L., and Starling, K. E. (1988). Generalized multiparameter correlation for nonpolar and polar fluid transport properties. *Industrial & engineering chemistry research*, 27(4):671–679.

Karellas, S. and Schuster, A. (2010). Supercritical fluid parameters in Organic Rankine Cycle applications. *International Journal of Thermodynamics*, 11(3):101–108.

Saleh, B., Koglbauer, G., Wendland, M., and Fischer, J. (2007). Working fluids for low-temperature Organic Rankine Cycles. *Energy*, 32(7):1210–1221.

Setzmann, U. and Wagner, W. (1989). A new method for optimizing the structure of thermodynamic correlation equations. *International Journal of Thermophysics*, 10(6):1103–1126.

Thompson, P. (1971). A Fundamental Derivative in Gas Dynamics. *Physics of Fluids*, 14:1843–1849.

Supercritical ORCs

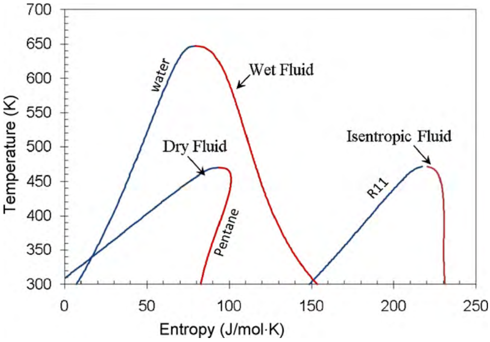

Saturated vapour curve slope for three different working fluids.
[Chen et al., 2010]

Criteria for the working fluid choice:

- Saturated vapour curve slope
- Fluid thermodynamic properties
- Cycle thermodynamic properties: enthalpy fall, turbine work, global efficiency;
- Turbine size
- Environmental properties
- Economic criteria
- Knowledge of an accurate EoS

Candidate working fluids: R134a, R245fa, CO_2

Fluid name	*Molar mass* (g/mol)	T_c (K)	p_c (kPa)	ρ_c (mol/L)
R134a	102.032	374.21	4059.28	5.017
R245fa	134.048	427.16	3651.0	3.85
CO_2	44.01	304.13	7377.3	10.625